Topological Effects on Globular Protein-ELP Fusion Block Copolymer Self-Assembly

*Guokui Qin, Matthew J. Glassman, Christopher N. Lam, Dongsook Chang, Eric Schaible, Alexander Hexemer, and Bradley D. Olsen**

Perfectly defined, monodisperse fusion protein block copolymers of a thermoresponsive coil-like protein, ELP, and a globular protein, mCherry, are demonstrated to act as fully biosynthetic analogues to protein-polymer conjugates that can self-assemble into biofunctional nanostructures such as hexagonal and lamellar phases in concentrated solutions. The phase behavior of two mCherry-ELP fusions, E_{10}-mCherry-E_{10} and E_{20}-mCherry, is investigated to compare linear and bola fusion self-assembly both in diluted and concentrated aqueous solution. In dilute solution, the molecular topology impacts the stability of micelles formed above the thermal transition temperature of the ELP block, with the diblock forming micelles and the bola forming unstable aggregates. Despite the chemical similarity of the two protein blocks, the materials order into block copolymer-like nanostructures across a wide range of concentrations at 30 wt% and above, with the bola fusion having a lower order-disorder transition concentration than the diblock fusion. The topology of the molecule has a large impact on the type of nanostructure formed, with the two fusions forming phases in the opposite order as a function of temperature and concentration. This new system provides a rich landscape to explore the capabilities of fusion architecture to control supramolecular assemblies for bioactive materials.

1. Introduction

Optically active proteins and enzymes are becoming increasingly attractive for biocatalytic and bioelectronic devices due to their substrate specificity and selectivity, high catalytic rates, and ability to operate under mild conditions.[1] Engineering these proteins into functional catalysts is enabling applications such as biosensors, environmentally friendly catalysts, and biofuel synthesis. The market for biocatalysts is well established with applications such as glucose-fructose conversion, pharmaceutical synthesis, and glucose sensing.[2] Engineering and improving heterogeneous biocatalysts for these applications requires achieving a high enzyme density; maintaining rapid transport of substrate, product, and charge carriers into and out of the active site; and controlling enzyme orientation to allow easy substrate access.[3] Analogous to synthetic catalysts,[4] this necessitates the arrangement of the protein into three-dimensional nanostructures with continuous transport pathways and controlled protein orientation at the interface of these pathways.[5]

Among a variety of different approaches to protein immobilization or encapsulation,[6,7] the self-assembly of block copolymers containing an enzyme or optically active protein block presents an opportunity to engineer a biomaterial that simultaneously achieves multiphase structure, a high density of protein, and the correct protein orientation. This could then provide a bottom-up method for fabricating nanopatterns in three dimensions that may be of high value for producing enzyme-based materials.[8] Block copolymers containing polypeptide blocks are well known to self-assemble into a wide variety of nanostructures with characteristic length scales from 5 to 100 nm, where the secondary structure of the protein has a large impact on self-assembly.[10] Incorporating a globular protein as one block in a block copolymer changes the thermodynamics of self-assembly due to the folded shape of the protein domain and specific interactions between proteins.[9–14] Recently, the self-assembly of mCherry-PNIPAM conjugates has been studied in detail, demonstrating complex phase diagrams as a function of concentration that include reentrant ODTs and a number of OOTs.[12,15] The phase diagram of mCherry-PNIPAM conjugates is highly asymmetric with predominantly hexagonal cylinders below a coil fraction of 0.5 and lamellar nanostructures above a coil fraction of 0.5.[15] Comparisons of mCherry and EGFP block copolymer self-assembly showed that diblock copolymer systems with structurally similar proteins have similar phase behavior.[12,13] However, changing the chemistry of the polymer block has a large impact on the type of ordered phases formed.[16] In addition, the position of the ODT concentration and the effect of changing polymer chemistry on this concentration suggest that protein-polymer repulsive interactions are important for self-assembly.[9,12–14]

Dr. G. Qin, M. J. Glassman, C. N. Lam, D. Chang, Prof. B. D. Olsen
Department of Chemical Engineering
Massachusetts Institute of Technology
77 Massachusetts Avenue
Cambridge, MA 02139, USA
E-mail: bdolsen@mit.edu
Dr. E. Schaible, Dr. A. Hexemer
Advanced Light Source
Lawrence Berkeley National Laboratory
1 Cyclotron Road, Berkeley, CA 94720, USA

DOI: 10.1002/adfm.201403453

Despite continued advances in bioconjugation chemistry,[17] protein-synthetic hybrid block copolymers are challenging to prepare due to the difficulty of performing site-specific, high yield bioconjugation, which limits the range of applications of these materials. Fusion proteins offer the opportunity to overcome the synthetic limits of bioconjugation by genetically encoding the entire block copolymer. Previous studies have shown the possiblity of creating self-assembled systems with new properties by combining two structural protein elements,[18,19] and the self-assembly of fusions between elastin-like polypeptides and globular proteins into micelles or aggregated nanoparticules in solution has been explored.[7,20–23] In addition, the feasibility of large scale purification of specifically designed fusion proteins has been demonstrated. For example, proteins can be purified as fusions with ELPs by inverse transition cycling (ITC), where the thermosensitive solubility imparted by the ELP tag allows for large scale purification of fusion proteins at low cost.[21,24,25]

Herein, it is demonstrated that fusion proteins of a coil-like protein ELP and a model globular protein mCherry can self-assemble into high density, solid-state biofunctional nanostructures as fully biosynthetic analogues of protein-polymer conjugate block copolymers. Using fusion purification tags, the block copolymers can be isolated at low cost, providing an integrated route to protein purification and self-assembly into solid, bioactive materials.[22,26] The self-assembly of fusion proteins in concentrated solutions and solid gels is explored, demonstrating the ability to undergo protein-protein microphase separation even in the absence of specific interactions between proteins. The phase behavior of the material is mapped in detail, showing order-disorder transitions (ODTs) and order-order transitions (OOTs) for the first time in fusion block copolymers. The effect of chain topology on self-assembly is explored by comparing a two tailed bola structure and a classical diblock structure, illustrating the powerful effect of genetic engineering to control self-assembly without changing polymer molar mass or composition.

2. Results and Discussion

To investigate the fundamental structure and thermodynamics of fusion block copolymers, model block copolymers were developed containing a globular protein and a coil-like protein by artificial protein engineering. A red fluorescent protein, mCherry, was used as a model globular protein, which was fused with structural elastin-like-polymers (ELPs) by genetic engineering to generate a new fusion protein system, mCherry-ELP. The role of shape can be explored by changing the sequence of blocks encoded through gene design. By fusing ELPs to both the N and C termini or the N terminus alone, E_{10}-mCherry-E_{10} and E_{20}-mCherry were prepared. Both have a weight fraction of mCherry ($f_{mCherry}$) = 0.4, but the molecules are constructed in either a diblock or double tail triblock architecture (**Figure 1**a). In the globular protein-polymer block copolymer, ELP chains are solvated and unstructured at low temperatures, but exhibit an inverse thermal transition and become insoluble at high temperatures.[27] mCherry-ELP fusions were expressed in *Escherichia coli* (*E. coli*) in soluble

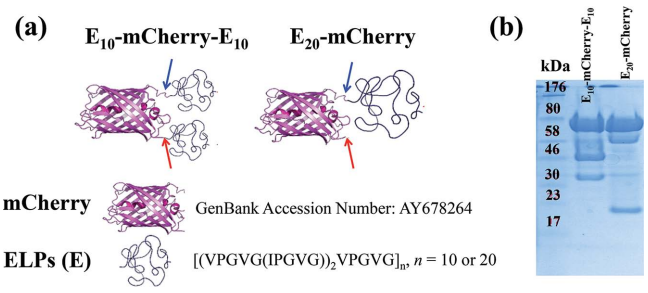

Figure 1. a) Schematic of mCherry-ELP fusion block copolymers for double and single tailed fusions. Red and blue arrows indicate the N and C termini, respectively. b) SDS-PAGE shows the purification of mCherry-ELP fusions expressed in *E. coli* cells. The two smaller molar mass bands in each lane which sum to the total molar mass of the parent protein are the result of the chromophore acylimine bond breaking during protein boiling under denaturing gel conditions.[9]

form with a yield of about 50 mg/L (Figure 1b and Supporting Information Figure S5). The T_t of the elastin was used to selectively precipitate and purify the fusion protein, allowing low-cost, self-assembling block copolymer materials to be easily produced. The relative ease of large-scale biosynthesis and purification, as well as the perfect control over block ratios, molecular architecture, and monodispersity make this protein fusion system well-suited for nanomaterial design.

2.1. Phase Behavior in Dilute Solution

The thermal transition properties of elastin-like peptides (ELPs) can trigger important strucutral transitions upon fusion to other proteins.[25,28] In E_{10} and E_{20} single block proteins, the thermal transitions are observed by turbidimetry and occurred at 36.2 °C and and 29.4 °C, respectively (Figure S6e,f, Supporting Information), at a concentration of 0.5 mg/mL. These results are consistent with several previous studies that show that the thermal transition of ELPs increases as the molar mass of the protein is decreased.[21,25,29] When the ELP is fused to mCherry, the solution behavior of mCherry-ELP fusions shows a strong dependence upon the shape of the molecule. Both fusions exist as isolated molecules in dilute solution below the ELP thermoresponsive transition temperature as indicated by dynamic light scattering (DLS) and turbidimetry (**Table 1**). The increase in turbidity for E_{10}-mCherry-E_{10} occured at a significantly lower temperature than for E_{20}-mCherry at equal protein concentration. The transition occurred at 36.4 °C for E_{10}-mCherry-E_{10} at 0.5 mg/mL and 23.4 °C at 10 mg/mL, similar to the E_{10} single block protein at the same concentration. In contrast, no obvious transition was observed for E_{20}-mCherry at 0.5 mg/mL, and only a small drop in transmission was observed at 10 mg/mL above 32.5 °C (Figure S6a–d, Supporting Information).[18]

Dynamic light scattering (DLS) and small-angle neutron scattering (SANS) show that the difference in turbidity between the two fusions is due to the fact that E_{10}-mCherry-E_{10} forms large aggregates above the thermoresponsive transition, while E_{20}-mCherry forms micelles. Table 1 shows both average particle sizes and measured polydispersities obtained by DLS above and below the responsive transition. Both mCherry-ELP fusions

Table 1. Molar mass, pI and average radius and mass fractions from DLS for mCherry-ELP fusions.

	Molar Mass [kDa]	pI	Hydrodynamic Radius (20 °C)	Hydrodynamic Radius (50 °C)
E_{10}-mCherry-E_{10}	70.3	5.4	7.1 nm	130.7 nm (40%) 263.5 nm (60%)
E_{20}-mCherry	69.4	5.5	5.7 nm	33.3 nm

have hydrodynamic radii of 6–7 nm at 20 °C, indicating that they are unaggregated at this temperature in dilute solution. When the temperature is increased up to 50 °C, E_{10}-mCherry-E_{10} reversibly forms 100 – 300 nm aggregates, where the characteristic dimension is much larger than the molecular size. In contrast, E_{20}-mCherry forms particles with a hydrodynamic radius of 33 nm, consistent with micelles.

SANS for both conjugates clearly shows that E_{20}-mCherry forms micelles while E_{10}-mCherry-E_{10} forms large, macrophase separated aggregates. **Figure 2** shows the difference in solution structure between these two designed architectures of the mCherry-ELP fusions. The experiments on 1% solutions demonstrate that despite having similar scattering patterns at low temperature (5 °C), the singly tailed fusion assembles into micelles with a regular shape and low polydispersity at high temperature (35 °C). However, the large increase in scattering intensity at low q for the doubly tailed fusion suggests large scale aggregation, consistent with observations from DLS and turbidimetry. As shown in Figure 2, at low temperature both fusions exhibit a Guinier regime, and Guinier analysis

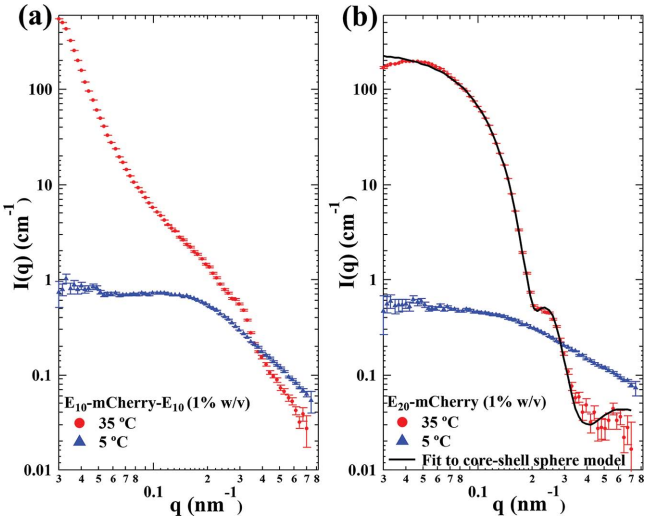

Figure 2. SANS studies for a) E_{10}-mCherry-E_{10} and b) E_{20}-mCherry showing individual molecules below T_t and molecular aggregates above T_t.

(Figure S7, Supporting Information) gives a radius of gyration of 4.7 ± 0.2 nm and 6.3 ± 0.2 nm for E_{10}-mCherry-E_{10} and E_{20}-mCherry, respectively. At high temperature, the micellar scattering signature of the singly tailed fusion protein E_{20}-mCherry was fit to a form factor model for spherical particles with a polydisperse core and a constant shell thickness.[30] The agreement between the experiment and model is good except at very low q, where the experimental scattering intensity drops slightly suggesting minor structure factor effects due to micelle interactions that are not captured in the isolated scatterer model. Based on the fitting results, the average core radius of E_{20}-mCherry is 18.2 ± 0.2 nm and the shell thickness is 17.8 ± 0.1 nm, so the average radius of E_{20}-mCherry particles is around 26 nm, in agreement with DLS studies.

2.2. Phase Behavior in Concentrated Solution

When self-assembled in concentrated solution above an order-disorder transition concentration (C_{ODT}) and below the ELP thermoresponsive transition temperature, both fusion proteins form ordered nanostructures reminiscent of traditional block copolymers. Ordered nanostructures formed by both conjugates in concentrated solutions and solid gels clearly indicate that protein blocks can microphase separate from one another even in the absence of quaternary structure forming interactions (i.e., crystallization to form β-fibrils or association of capsid proteins) that lead to protein aggregation or self-assembly and under conditions where both blocks are highly soluble.[23] The self-assembly process reported here is similarly interesting from the polymer science perspective, as both blocks have very similar compositions and therefore might be expected to have a mixing parameter that is nearly zero.

At concentrations below 30 wt%, both mCherry-ELP fusions form homogenous solutions at low temperature, while under more concentrated conditions nanostructured phases can be observed (**Figure 3**,**4** S8,S9). In E_{10}-mCherry-E_{10}, a disordered phase is observed at 20 wt% at low temperature, as evidenced by a single broad peak in SAXS. Increasing concentration to 30 wt% at temperatures below 20 °C yields a hexagonal phase with clearly resolved q^*, $\sqrt{3}q^*$, $\sqrt{4}q^*$, $\sqrt{7}q^*$, $\sqrt{9}q^*$, $\sqrt{12}q^*$, and $\sqrt{13}q^*$ peaks. Increasing concentration further to 55 wt% at low temperature changes the nanostructure to lamellar with peaks at q^* and $2q^*$ (Figure 3a). The peaks broaden with further increasing concentration to 60 wt%, suggesting that the degree of order decreases. E_{20}-mCherry forms significantly different nanostructures at temperatures below T_t. It remains disordered below 40 wt%, at which point a lamellar phase is observed with peaks at q^*, $2q^*$, $3q^*$ (Figure 3b). At 40 wt% the primary peak is superimposed on a broad scattering feature, suggestive of coexistence between lamellar and disordered phases; this disorderd phase disappears at higher concentration. When increasing concentration to 45 wt%, a doubled primary peak q^* is observed with two clearly resolvable $2q^*$ peaks, indicating coexistence between two lamellar phases with different domain spacing (Figure S10, Supporting Information). At 50 wt% and above only the second lamellar phase with larger domain spacing is observed, and the material begins to disorder again upon further increasing concentration to 60 wt%. These results clearly

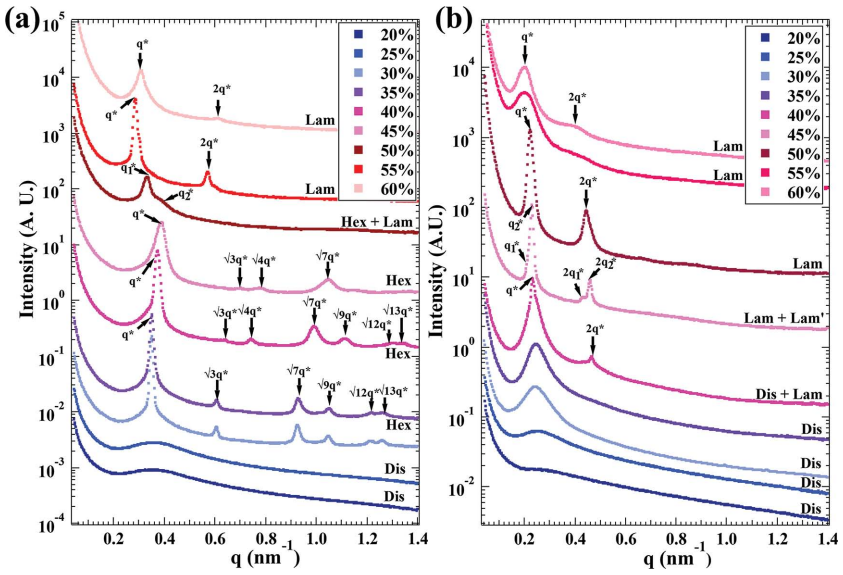

Figure 3. SAXS patterns of fusion proteins as a function of concentration (20–60 wt%) at 10 °C for a) E_{10}-mCherry-E_{10} and b) E_{20}-mCherry. The curves are offset for clarity.

indicate that the topology of the block copolymer has a large impact on both the C_{ODT} and the type of nanostructure formed, with the bola molecule demonstrating a lower C_{ODT} and better ordered nanostructures across a wide range of concentration.

Phase diagrams for both conjugates (Figure 4) as a function of temperature and concentration show that changes in ELP solvation with temperature induced order-order transitions (OOTs) in the fusion protein materials both above and below the T_t of the ELP. Phase diagrams are assembled using a combination of DSC, turbidimetry, DPLS, and SAXS to identify the phase transitions and ordered structures (**Table 2**), providing insight into the nature of the structural transitions and the effects of molecular topology. Despite having identical composition, there are large differences in the order-disorder and order-order transitions for these two proteins related to the molecular topology.

Below the low temperature C_{ODT}, both fusion proteins display different ELP desolvation-induced ordering transitions above an order-disorder transition temperature (T_{ODT}). For concentrations of 30 wt% and below, an endothermic transition peak can be seen for E_{10}-mCherry-E_{10} by DSC at ≈33 °C due to desolvation of the ELP chains in the fusion block copolymers (Table 2). This transition corresponds to a macrophase separation transition, which at 20 and 25 wt% is a transition from a low temperature disordered phase to a high temperature two phase region with a lamellar conjugate-rich phase and a conjugate-poor phase. The high temperature phase is identified baesd upon a large increase in turbidity, indicating macrophase separation, and a lamellar peak pattern in SAXS. A similar endothermic transition is observed for E_{20}-mCherry at ≈28 °C for concentrations of 25 wt% and below. In this conjugate, the

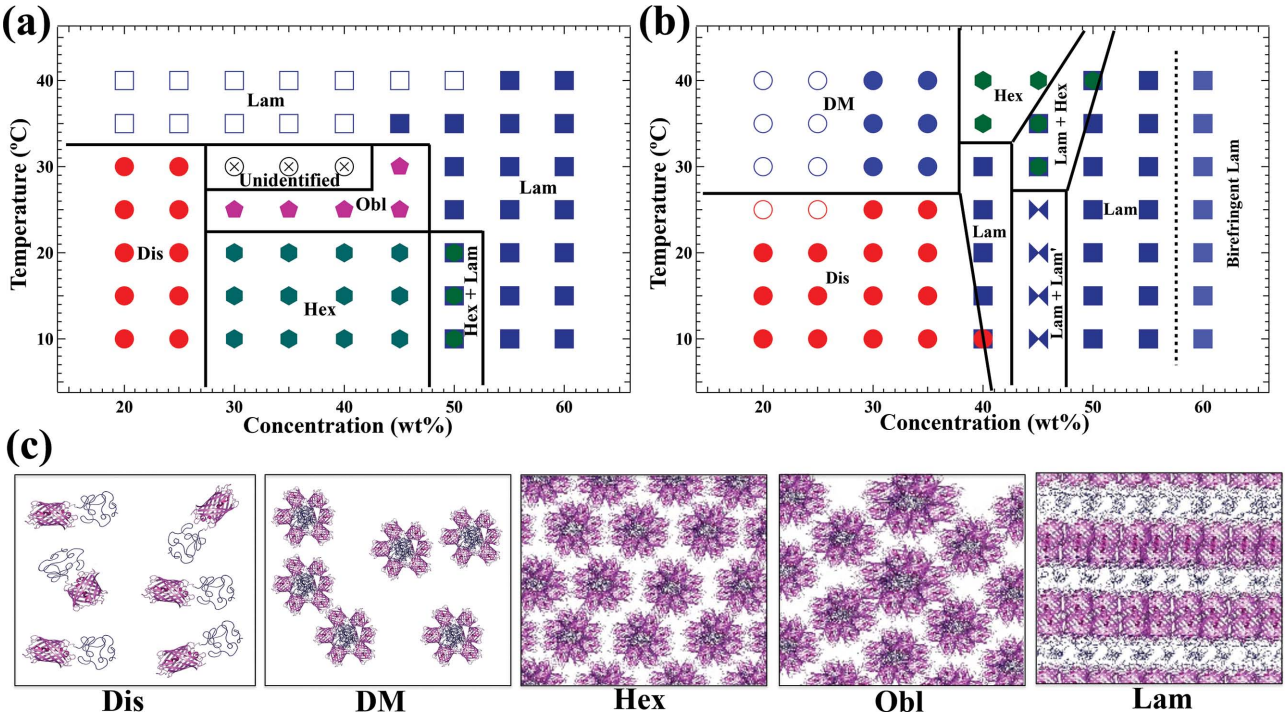

Figure 4. Phase diagrams of fusion proteins as a function of temperature and concentration for a) E_{10}-mCherry-E_{10} and b) E_{20}-mCherry. The various phases are denoted as disordered (Dis), disordered micellar (DM), hexagonal (Hex), oblique (Obl) and lamellar (Lam) as shown in (c). Open symbols represent regions where macrophase separation between a fusion-rich phase and a water-rich phase is observed.

Table 2. Thermal transitions for mCherry-ELP fusion systems as measured by DPLS, turbidimetry, and DSC.

Sample	Conc. [wt%]	T_{DPLS} [°C]	T_t [°C]	T_{DSC} [°C]
E_{10}-mCherry-E_{10}	20	□	31.5	33
	25	□	32.9	34
	30	□	33.1	35
	35	□	34.1	/
	40	□	35.1	/
	45	□	36.6	/
	50	□	39.4	/
	55	□	/	/
	60	□	/	/
E_{20}-mCherry	20	□	21.6	28
	25	□	23.2	29
	30	□	/	/
	35	□	/	/
	40	□	/	/
	45	□	/	/
	50	□	/	/
	55	□	/	/
	60	■	/	/

□ denotes samples that never display birefringence, ■ denotes samples that remain birefringent at all temperatures, and / denotes samples in which thermal transitions are not observed.

transition corresponds to a change from a low temperature disordered phase to a high temperature two phase region with a disordered micellar conjugate-rich phase and a conjugate-poor phase. In this case, the turbidity is observed as low as 25 °C, suggesting two phase structure before disordered micelles are observed by SAXS. The transition between disordered and disordered micellar structures persists at 30 and 35 wt%, but the high temperature micellar phase observed at 30 °C and above is now homogeneous. The formation of the lamellar phase for E_{10}-mCherry-E_{10} as compared to disordered micellar phases for E_{20}-mCherry and all previous diblock protein conjugates suggests a strong suppression of curvature due to the addition of multilple tails in the bola fusion.[12,13]

As each fusion is increased above its low temperature C_{ODT}, the differences between the two molecular topologies become more pronounced. With increasing concentration, E_{10}-mCherry-E_{10} first enters an ordered region from 30 to 45 wt% where it transitions from a hexagonal to an oblique to a lamellar phase upon increasing temperature; representative SAXS patterns for these different phases are shown in **Figure 5**a. The transition from the hexagonal phase (peaks at q^*, $\sqrt{3}q^*$, $\sqrt{7}q^*$, $\sqrt{9}q^*$, $\sqrt{12}q^*$, and $\sqrt{13}q^*$) to the oblique phase (peaks indexed as 100, 010, 110, 200, 210, $3\bar{1}0$, $\bar{2}30$, 310, and 130) occurs between 20 and 25 °C (Table S2, Supporting Information). At 30 °C there is a narrow region of a phase that is well-ordered as indicated by several sharp peaks in SAXS, but does not match any of the known block copolymer structures and has too few peaks to be reliably indexed; above this temperature the material transitions into a macrophase separated lamellar structure as evidenced by a dramatic increase in turbidity and SAXS peaks at q^*, $2q^*$, and $4q^*$. This sequence of transitions is consistent with the formation of an ELP continuous phase in the hexagonal structures at low temperature which collapses to yield an eventual high temperature lamellar phase. The oblique structures can be formed at intermediate temperatures by shifting the planes of cylinders in the hexagonal phase closer together along one dimension due to desolvation of the ELP domain.

Increasing concentration to 55 wt% and above in the E_{10}-mCherry-E_{10} fusion also yields a transition to a lamellar phase, as evidenced by SAXS peaks at integer multiples of the primary peak spacing. At these high concentrations, the material remains in a single lamellar phase across all temperatures, although changes in ELP solvation are manifest through changes in the lamellar form factor that modulates the relative peak intensities in the SAXS pattern. At high temperature, the primary scattering peak is reduced in intensity without accompanying shifts in any of the peak positions, suggesting that the form factor of the lamellae changes without changing the symmetry or domain spacing of the phase. At 40 °C, the primary peak disappears entirely. This effect is consistent with the exclusion of water from the ELP domains into the mCherry domains with heating. Because the mCherry domains cannot change chain configuration upon swelling with water, water can segregate inhomogeneously into the domains, presumably near the center of the domain. This arrangement of water can yield a lamellar form factor with a minimum overlapping the primary peak from the structure factor. Dividing the lamellar and hexagonal regimes is a narrow coexistence region at 50 wt%, where increasing temperature results in a transition from a low temperature lamellar/hexagonal coexistence region to a high temperature lamellar phase. Despite the well-resolved and sharp scatteirng peaks across much of the phase diagram, none of the

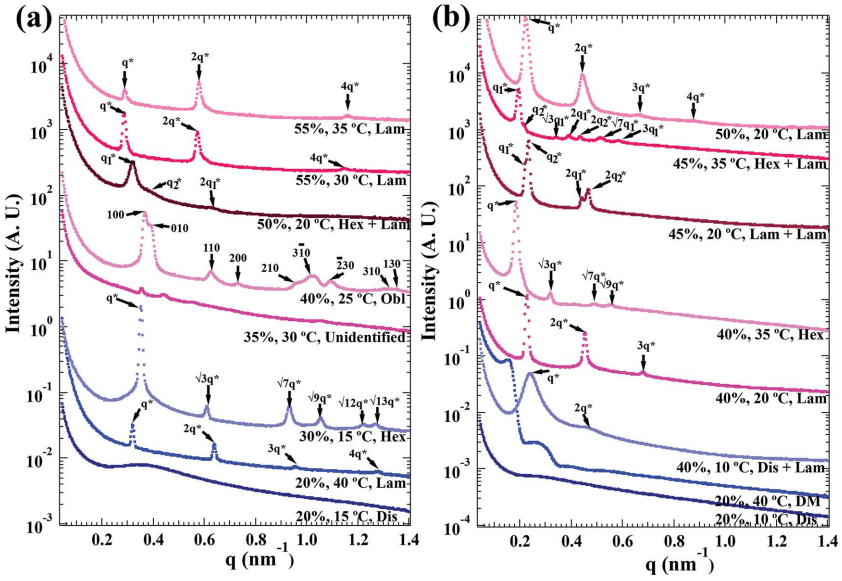

Figure 5. Representative SAXS patterns for a) E_{10}-mCherry-E_{10} and b) E_{20}-mCherry illustrating all different phases observed in each fusion. The curves are offset for clarity.

phases exhibit birefringence; a significant contributing factor may be relatively low refractive index contrast between the two blocks of the copolymer due to the high chemical similarity.

Compared to E_{10}-mCherry-E_{10}, E_{20}-mCherry has significantly different phase behavior in the ordered region of the phase diagram (Figure 4b, 5b). Just above the ODT at 40 wt%, a narrow lamellar region is observed, with a transition to a hexagonal phase observed upon ELP chain desolvation at 35 °C and above. This hexagonal phase presumably contains protein as the continuous phase due to chain collapse of the ELP. At 50 wt% and above a larger domain spacing lamellar structure is formed across a wide range of temperatures. A narrow region of lamellar-lamellar coexistence between the large and small domain phases is observed at 45 wt% below 35 °C. At 35 °C and above, this region transitions into a lamellar-hexagonal coexistence region at 45 wt%, extending at 40 °C out to 50 wt%. Despite sharp peaks observed in the SAXS patterns, none of the ordered phases is birefringent until 60 wt%, where the lamellar phase becomes birefringent throughout the entire experimental temperature range.[12,13]

In comparison to the E_{10}-mCherry-E_{10} bola fusion with different concentrations and temperatures, the E_{20}-mCherry diblock fusion has a larger domain spacing range as measured by SAXS (Figure S10, Supporting Information), suggesting the less interfacial per molecule in the E_{20}-mCherry diblock fusion. This effect is consistent with different shape parameters for the two molecules and the observation that in the bola fusion the ELP tends to form the continuous domain in hexagonal phases while in the diblock fusion the ELP tends to form the discrete domains. At low concentration, heating through the T_t of the ELP block results in a discontinuous increase in domain spacing due to increasing strength of segregation between blocks in a selective solvent. However, at high concentration, little change of domain spacing is observed for both funsions as a function of temperature. In all cases, as the temperature is increased up to 40 °C, the domain spacing for both fusions converges to a small number of values corresponding to the different high temperature phases.

Because of the similar molecular structure of the fusion proteins (particularly E_{20}-mCherry) to protein-polymer conjugates, comparisons with previously reported studies of self-assembly in hybrid protien-synthetic systems are natural. This comparison reveals a set of common features observed in their concentrated solution phase behavior.[31] Conjugates of mCherry with three different thermoresponsive polymers—poly(N-isopropylacrylamide) (PNIPAM), poly(hydroxypropyl acrylate) (PHPA), and poly(oligoethylene glycol acrylate) (POEGA)—form isotropic solutions at low concentration and temperature and disordered micellar structures at high temperatures above the polymers' thermoresponsive transition point. With increasing concentration, these model mCherry-polymer bioconjugates all form well-ordered nanostructures with a C_{ODT} between 30 and 45 wt% for symmetric conjugates. Interestingly, with a further increase in concentration, these protein-polymer bioconjugates undergo a reentrant order-disorder transition.[31] As seen in Figure 4, many of these features are observed in the fusion proteins as well, including a low concentration, low temperature disordered phase transitioning to a disordered micellar phase at high temperature, a range of concentrations between which the fusion protein self-assembles into long-ranged ordered nanostructures, and a decrease in order with increasing concentration. However, E_{20}-mCherry, which has the same molecular topology as the protein-polymer conjugates, is not observed to form a perforated lamellar or a cubic phase as has been observed previously in all of the symmetric protein-polymer conjugates.[31] Therefore, the change from synthetic polymer to ELP is directly analagous to a change in polymer chemistry, yielding little change in the overall shape of the phase diagram but significant changes in the ODT, OOT, and type of nanostructures formed.

While the phase behaviors of both ELP-mCherry fusion proteins show common features and form similar phases to those observed in protein-polymer conjugates with synthetic polymer blocks, the difference in topology between these two fusion proteins leads to differences in phases and locations of phase transitions observed. The E_{10}-mCherry-E_{10} bola fusion has a C_{ODT} of approximately 30 wt%, 10 wt% lower than that of E_{20}-mCherry. Therefore, changing chain topology can provide a stronger driving force for self-assembly without changing molecular composition. It is hypothesized that this difference occurs because the change in chain topology minimizes the chain stretching penalty of the ELP block for self-assembly. Unlike all previously studied diblock fusions or conjugates, the bola fusion forms a lamellar phase above the ELP T_t and at low concentration instead of a disordered micellar phase. Furthermore, the low temperature lyotropic C_{ODT} is a transition from a disordered to a hexagonally packed morphology; further increasing concentration or temperature induces lyotropic or thermotropic transitions to lamellar phases. This is opposite to the typical order of phase transitions observed in the linear E_{20}-mCherry fusion and the previously studied linear protein-polymer conjugates, where the first ordered phase observed above the C_{ODT} is typically a lamellar phase, which then undergoes a thermotropic or lyotropic OOT to a hexagonal phase due to dehydration of the thermoresponsive polymer at high temperatures or decreasing hydration with increasing bioconjugate concentration. The opposite direction of the transition implies that the hexagonal phase observed in the bola structure has an ELP continuous domain such that desolvation of the ELP results in transition to a lamellar structure. This difference in the phases indicates that tuning the shape parameter of the fusion proteins through the addition of multiple coil-like protein tails[23] is a powerful method for tuning the thermodynamics of self-assembly.

2.3. Preservation of Function and Secondary Structure

Molecular design and processing conditions have a large effect on the function of protein in self-assembled nanostructures. Using UV–Vis spectroscopy to monitor the mCherry chromophore provides a sensitive probe for the maintenance of protein fold and function in solid materials and gels that is independent of transport considerations. Spectra for mCherry alone, E_{10}-mCherry-E_{10} and E_{20}-mCherry in **Figure 6**a show that both fusions, as expressed, have diminished mCherry absorbance. The fusion of E_{10}-mCherry-E_{10} preserved the highest levels of protein function, with 90% of the original

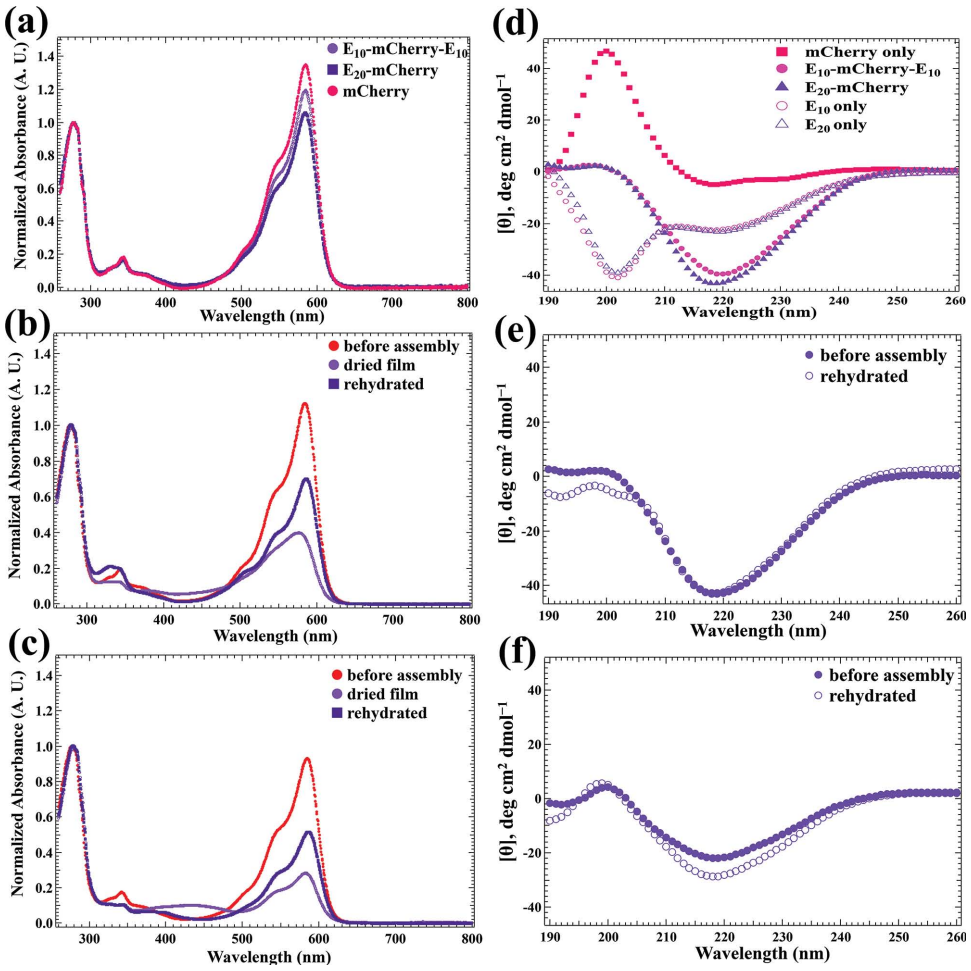

Figure 6. Protein absorbance spectra for a) E_{10}-mCherry-E_{10}, E_{20}-mCherry and mCherry, and the dehydrated and rehydrated samples for b) E_{10}-mCherry-E_{10} and c) E_{20}-mCherry. d) CD studies of E_{10}-mCherry-E_{10}, E_{20}-mCherry and mCherry alone, and the dehydrated and rehydrated samples for e) E_{10}-mCherry-E_{10} and f) E_{20}-mCherry, showing no large change of secondary structures.

solution-state absorbance preserved, compare to 75% for E_{20}-mCherry. It is speculated that this drop in aborbance results from a decreased folding efficiency of the protein with the ELP blocks attached during expression in *E. coli*, as all purification was performed under native conditions and the folded protein is stable in solution. Solid-state samples cast on quartz disks (Figure 6b,c) show a substantial decrease in the peak absorption of the mCherrry chromophore at 586 nm. The protein retains 34% of its absorbance for E_{10}-mCherry-E_{10}, while only 30% is retained for E_{20}-mCherry. This loss could be due to dehydration of fusion proteins, which will affect the conformation of mCherry chromophore. Upon rehydration, the peak absorption at 586 nm increased to 66% of its original value for E_{10}-mCherry-E_{10} and 56% for E_{20}-mCherry, suggesting that there is a fraction of irreversibly inactivated chromophore in the fusion proteins. Therefore, there is a pronounced effect on the mCherry due to the topological difference between two fusion proteins with singly or doubly tailed ELP structures, with the double tail structure performing signifcantly better.

The retention of protein function in the fusion constructs is comparable to that observed in protien-polymer conjugates. A previous investigation of mCherry-PNIPAM bioconjugates has shown that the self-assembly process preserves a large fraction of the protein secondary structure and optical activity, even after having been dehydrated and rehydrated. mCherry conjugated to PNIPAM at a coil fraction of 0.66[9] and to PHPA and POEGA[16] as a function of coil fraction ($f_{polymer}$ = 0.4–0.7) have shown that after bioconjugation, the absorbance of the conjugate in solution is approximately 80–90% relative to that of unconjugated mCherry. By comparison, E_{20}-mCherry retains about 75% of the mCherry chromophore absorption after synthesis and purification, and E_{10}-mCherry-E_{10} retained 90% after purification. After self-assembly and rehydration, mCherry-PNIPAM retains 75–85% of its original function for volume fractions over the range of 0.42 to 0.69; therefore, the fusion constructs irreversibly lose somewhat more functionality upon solvent casting than the protein-polymer conjugates.[32]

The coil-like ELP chains increase the fraction of unordered secondary structure upon ELP fused within the block copolymer systems. CD spectra showed that the mCherry alone was composed of 46% β-sheets, while the mCherry-ELP fusion block copolymers in solution after purification were 30–34% β-sheets (Figure 6d). The percent of unordered structure increased to more than 40% for both fusions (Table S1,

Supporting Information). The high content of β-sheets in the fusion system also indicates no large change of secondary structure of globular protein mCherry in the whole mCherry-ELP fusion systems. CD spectra of the rehydrated fusions show very little change from the fusion proteins before self-assembly (Figure 6e,f), indicating that the majority of the protein retains identical secondary structure to the native protein, even after having been dehydrated and rehydrated.[14,32]

Both results from UV–Vis and CD studies confirmed that, despite changes in protein function with topological effects, the secondary structure is largely preserved for both singly or doubly tailed mCherry-ELP fusions, showing predominantly β-sheet structure with the same β-sheet content. While protein secondary structure retention is required to maintain high levels of protein functionality, changes in tertiary structure also contribute to overall protein function. The results above suggest that the tertiary structure of the globular protein is disrupted at different levels based on different designs from our fusion proteins, resulting in an irreversible loss of function ranging from 34 to 44% of the total globular protein. However, the degree of function retained is remarkably high compared to most enzyme immobilization methods, making this an attractive route to preserve biological activity in nanostructured systems.

3. Conclusion

Fusion proteins of a model globular protein (mCherry) and a coil-like protein (ELPs), the fully biosynthetic analogue to protein-polymer block copolymer systems, are demonstrated for the first time to self-assemble into nanostructured block copolymer-like materials in concentrated solution, even under conditions where both blocks are soluble and in the absence of quaternary structure forming interactions between proteins. Genetic engineering of the block copolymer constructs enables the comparison of two different molecular architectures, E_{10}-mCherry-E_{10} bola fusions and E_{20}-mCherry diblock fusions. In dilute solution, the ELP thermal transition temperature triggers self-assembly, with the single tail fusion exhibiting a lower T_t and the formation of micelles, while the double tail fusion shows a higher T_t and macrophase separation. During self-assembly at concentrations below 30 wt%, both mCherry-ELP fusions form homogenous solutions at low temperature, while under more concentrated conditions nanostructured phases can be observed with the bola fusion having a lower order-disorder transition concentration than the diblock fusion. In the range of 40–60 wt%, the different OOTs with increasing temperature were found for the different fusions due to desolvation of the ELP block. In E_{20}-mCherry this transition is from lamellar to hexagonal, while in E_{10}-mCherry-E_{10} this transition is from hexagonal to lamellar, with an intermediate oblique phase observed. Finally, the doubly tailed mCherry-ELP fusion demonstrated significantly better protein function preservation in the solution state than the singly tailed fusion, but with the similar secondary structure. Not only do the fusion proteins described here provide important new insight into the effect of chain topology in block copolymer self assembly with globular proteins, but they also provide a low cost, robust method to purify proteins and fabricate nanostructures in one integrated process. Therefore, these self-assembled fusions provide a rich landscape to explore the capabilities of protein design to control supramolecular assemblies for cost-effective heterogeneous biocatalysts and other biofunctional materials.

4. Experimental Section

Sample Preparation: Complete biosynthesis procedures and sequences for mCherry-ELP fusions are provided in the Supporting Information (Figure S1–S5, Supporting Information). Fusion protein solutions, dialyzed into pure water, were concentrated to approximately 100 mg/mL using Millipore Ultra-15 centrifugal filters with a molecular weight cutoff of 10 kDa. The fusion proteins were then diluted to different concentrations with concentration confirmed using an Implen Nanophotometer (Implen GmbH, Germany). Self-assembly of mCherry-ELP fusion block copolymers was accomplished through evaporation of water from fusion protein solutions to form nanostructured materials. The concentrated solutions were cast in 20 µL aliquots on a Teflon sheet and gradually exposed to vacuum at a ramp rate of 50 Torr/h and held at 10 Torr overnight at room temperature. The pellets were re-dissolved in water to prepare desired concentrations of sample solutions and equilibrated at 4 °C at least overnight.

Phase Transitions: To confirm whether the mCherry-ELP fusions still preserve the thermal responsive properties of ELPs, the changes in the optical density (OD) of protein solutions at 700 nm were first investigated on a Cary 50 UV–Vis spectrophotometer with a Peltier temperature controller using a quartz cuvette. Reversibility of the transition was examined by heating and cooling at 1 °C/min over the range 10–50 °C. The transitions were defined as the temperatures corresponding to a 10% reduction in the initial sample transmittance, according to previous methods.[13,33] Dynamic light scattering (DLS) experiments were then performed at 20 °C and 50 °C on a DynaPro Nanostar at a scattering angle of 90°, with a laser wavelength of 658 nm. Differential scanning calorimetry (DSC) was performed on a TA Instruments Q-10. Fusion proteins were loaded into hermetically sealed aluminium pans and cycled twice at 10 °C/min over the range 10–50 °C. Transition temperatures (T_t) were determined from the peak position on the second heating cycle. Turbidimetry and depolarized light scattering (DPLS) were performed on samples loaded into a 1 mm thick Teflon mold and sealed between two quartz disks. A Coherent OBIS LX660 laser with wavelength 662 nm was used to perform measurements above the bandgap of mCherry. The static birefringence and turbidimetry of fusion protein samples were collected and analyzed over the temperature range of 10–40 °C.[12,13]

Small-Angle Neutron Scattering (SANS): SANS experiments were performed at the High Flux Isotope Reactor (HFIR) at the Oak Ridge National Laboratory at 10 and 35 °C. Absolute intensities were obtained by correcting for background scattering and open beam neutron flux. Samples were equilibrated for at least 30 min at each temperature. The scattering spectrum for E_{20}-mCherry (1% w/v) at T = 35 °C was fit to a form factor for polydisperse spherical core–shell particles where the core is polydisperse, but the shell thickness is constant. The data were fit according to the NCNR SANS Reduction and Analysis procedures.[30] The fitting was performed and analyzed using the Igor pro software with the NCNR SANS analysis Igor macros.[30] Guinier analysis was performed using a weighted linear least squares algorithm as part of the KCL SAS Analysis Igor macro procedures provided by Oak Ridge National Lab.

Small-Angle X-Ray Scattering (SAXS): The prepared solutions were used to fill 1 mm thick anodized aluminum washers backed with Kapton tape. The washers were covered with Kapton tape to seal. The fusion proteins were measured on Beamline 7.3.3 of the Advanced Light Source (ALS) at Lawrence Berkeley National Lab, and some samples were also performed at NSLS beamline X9 at Brookhaven National Laboratory. Samples were equilibrated at 10 °C for 20 min and for 10 min at all other temperatures prior to data collection. SAXS data were collected

and corrected for empty cell and dark field scattering. Acquisition times were chosen such that the effect of beam damage on sample nanostructure was undetectable. All observed transitions were reversible with temperature.

Function Determination: UV–Vis spectra were collected on a Cary 50 UV–Vis spectrophotometer with a Peltier temperature controller using a quartz cuvette for protein solutions. Protein solution samples were vacuum dried on the quartz discs at a ramp rate of 50 Torr/h for comparison before and after material self-assembly, and the UV–Vis spectra of dried films were collected on quartz discs as previously shown.[14,32] The solid materials were then rehydrated to the designed concentrations for material characterization after self-assembly, and spectra were collected again. A spectrophotometric measure of protein function is calculated as A_{586} of the fusion sample relative to A_{586} of the mCherry control, where both values are normalized by A_{280} to control for variations in protein concentration. At least three replicates were averaged for each sample to produce the final data.

Secondary Structure: Fusion proteins were prepared as solutions (0.5–1 mg/mL) in water, and then loaded into a quartz cuvette with a 1 mm path length. Samples were scanned using an Aviv Model 202 Circular Dichroism (CD) Spectrometer with a Peltier temperature controller. CD spectra were collected with 1 nm resolution and an averaging time of 5 s and converted into molar ellipticity by correcting for the water background and using the concentration determined by the A_{280}. CD data deconvolution was analyzed using the DICHROWEB program.[34]

Supporting Information

Supporting Information is available from the Wiley Online Library or from the author.

Acknowledgements

This work was supported by National Science Foundation (award number DMR-1253306) and the Department of Energy Office of Basic Energy Sciences (award number DE-SC0007106). SANS experiments were performed at the High Flux Isotope Reactor (HFIR) at the Oak Ridge National Laboratory (ORNL). The research conducted at ORNL's HFIR was sponsored by the Scientific User Facilities Division, Office of Basic Energy Sciences, US Department of Energy. SAXS experiments were performed at ALS Beamline 7.3.3 at Lawrence Berkeley National Laboratory and NSLS beamline X9 at Brookhaven National Laboratory. We thank Dr. Chenhui Zhu (ALS) for experimental assistance with SAXS. CD and DLS were collected from Biophysical Instrumentation Facility at MIT. We also thank Shengchang Tang for help with UV–Vis studies and Charlotte Stewart-Sloan for help with DSC experiments performed at the Institute for Soldier Nanotechnologies (ISN).

Received: October 2, 2014
Revised: November 4, 2014
Published online: December 16, 2014

[1] a) I. Willner, *Science* **2002**, *298*, 2407; b) H. Krassen, A. Schwarze, B. Friedrich, K. Ataka, O. Lenz, J. Heberle, *ACS Nano* **2009**, *3*, 4055; c) T. Reda, C. M. Plugge, N. J. Abram, J. Hirst, *Proc. Natl. Acad. Sci. U.S.A.* **2008**, *105*, 10654; d) A. Schmid, J. S. Dordick, B. Hauer, A. Kiener, M. Wubbolts, B. Witholt, *Nature* **2001**, *409*, 258.

[2] a) B. Elleby, L. C. Chirica, C. K. Tu, M. Zeppezauer, S. Lindskog, *Eur. J. Biochem.* **2001**, *268*, 1613; b) P. Mirjafari, K. Asghari, N. Mahinpey, *Ind. Eng. Chem. Res.* **2007**, *46*, 921; c) O. B. Ayyub, M. B. Ibrahim, R. M. Briber, P. Kofinas, *Biosens. Bioelectron.* **2013**, *46*, 124; d) O. B. Ayyub, J. W. Sekowski, T. I. Yang, X. Zhang, R. M. Briber, P. Kofinas, *Biosens. Bioelectron.* **2011**, *28*, 349.

[3] a) R. Das, P. J. Kiley, M. Segal, J. Norville, A. A. Yu, L. Y. Wang, S. A. Trammell, L. E. Reddick, R. Kumar, F. Stellacci, N. Lebedev, J. Schnur, B. D. Bruce, S. G. Zhang, M. Baldo, *Nano Lett.* **2004**, *4*, 1079; b) I. Willner, E. Katz, *Angew. Chem. Int. Ed.* **2000**, *39*, 1180; c) I. Willner, B. Willner, *Trends Biotechnol.* **2001**, *19*, 222.

[4] a) E. E. Benson, C. P. Kubiak, A. J. Sathrum, J. M. Smieja, *Chem. Soc. Rev.* **2009**, *38*, 89; b) M. Mikkelsen, M. Jorgensen, F. C. Krebs, *Energy Environ. Sci.3*, 43.

[5] A. D. Presley, J. J. Chang, T. Xu, *Soft Matter* **2010**, *7*, 172.

[6] a) G. A. Becht, S. Lee, S. Seifert, M. A. Firestone, *J. Phys. Chem. B* **2010**, *114*, 14703; b) O. Green, S. Grubjesic, S. W. Lee, M. A. Firestone, *Polym. Rev.* **2009**, *49*, 339; c) S. Lee, G. A. Becht, B. Lee, C. T. Burns, M. A. Firestone, *Adv. Funct. Mater.* **2010**, *20*, 2063.

[7] a) M. A. Kostiainen, P. Hiekkataipale, J. A. de la Torre, R. J. M. Nolte, J. J. L. M. Cornelissen, *J. Mater. Chem.* **2011**, *21*, 2112; b) M. A. Kostiainen, C. Pietsch, R. Hoogenboom, R. J. M. Nolte, J. J. L. M. Cornelissen, *Adv. Funct. Mater.* **2011**, *21*, 2012.

[8] a) O. D. Krishna, K. L. Kiick, *Biopolymers* **2010**, *94*, 32; b) L. A. Canalle, D. Lowik, J. C. M. van Hest, *Chem. Soc. Rev.* **2010**, *39*, 329.

[9] C. S. Thomas, M. J. Glassman, B. D. Olsen, *ACS Nano* **2011**, *5*, 5697.

[10] a) J. T. Chen, E. L. Thomas, C. K. Ober, G. P. Mao, *Science* **1996**, *273*, 343; b) L. H. Radzilowski, B. O. Carragher, S. I. Stupp, *Macromolecules* **1997**, *30*, 2110; c) K. K. Tenneti, X. F. Chen, C. Y. Li, Y. F. Tu, X. H. Wan, Q. F. Zhou, I. Sics, B. S. Hsiao, *J. Am. Chem. Soc.* **2005**, *127*, 15481.

[11] a) M. J. Glassman, J. Chan, B. D. Olsen, *Adv. Funct. Mater.* **2013**, *23*, 1182; b) M. J. Glassman, B. D. Olsen, *Soft Matter* **2013**, *9*, 6814.

[12] C. N. Lam, M. Kim, C. S. Thomas, D. Chang, G. E. Sanoja, C. U. Okwara, B. D. Olsen, *Biomacromolecules* **2014**.

[13] C. N. Lam, B. D. Olsen, *Soft Matter* **2013**, *9*, 2393.

[14] C. S. Thomas, L. Xu, B. D. Olsen, *Biomacromolecules* **2012**, *13*, 2781.

[15] C. S. Thomas, B. D. Olsen, *Soft Matter* **2014**, *10*, 3093.

[16] D. Chang, C. N. Lam, S. Tang, B. D. Olsen, *Polym. Chem.* **2014**, *5*, 4884.

[17] a) M. H. Stenzel, *ACS Macro Lett.* **2013**, *2*, 14; b) J. Kalia, R. T. Raines, *Curr. Org. Chem.* **2010**, *14*, 138.

[18] X. X. Xia, Q. B. Xu, X. Hu, G. K. Qin, D. L. Kaplan, *Biomacromolecules* **2011**, *12*, 3844.

[19] a) L. Li, K. L. Kiick, *ACS Macro Lett.* **2013**, *2*, 635; b) S. Lv, D. M. Dudek, Y. Cao, M. M. Balamurali, J. Gosline, H. B. Li, *Nature* **2010**, *465*, 69.

[20] E. G. Bellomo, M. D. Wyrsta, L. Pakstis, D. J. Pochan, T. J. Deming, *Nat. Mater.* **2004**, *3*, 244; c) X. X. Xia, M. Wang, Y. A. Lin, Q. B. Xu, D. L. Kaplan, *Biomacromolecules* **2014**, *15*, 908.

[21] D. E. Meyer, A. Chilkoti, *Nat. Biotechnol.* **1999**, *17*, 1112.

[22] A. J. Simnick, D. W. Lim, D. Chow, A. Chilkoti, *Polym. Rev.* **2007**, *47*, 121.

[23] M. B. van Eldijk, J. C. Wang, I. J. Minten, C. Li, A. Zlotnick, R. J. Nolte, J. J. Cornelissen, J. C. van Hest, *J. Am. Chem. Soc.* **2012**, *134*, 18506.

[24] a) K. Trabbic-Carlson, L. Liu, B. Kim, A. Chilkoti, *Protein Sci.* **2004**, *13*, 3274; b) J. J. Bellucci, M. Amiram, J. Bhattacharyya, D. McCafferty, A. Chilkoti, *Angew. Chem. Int. Ed.* **2013**, *52*, 3703.

[25] K. Trabbic-Carlson, D. E. Meyer, L. Liu, R. Piervincenzi, N. Nath, T. LaBean, A. Chilkoti, *Protein Eng. Des. Sel.* **2004**, *17*, 57.

[26] a) Y. Xia, S. Tang, B. D. Olsen, *Chem. Commun.* **2013**, *49*, 2566; b) J. Hyun, W. K. Lee, N. Nath, A. Chilkoti, S. Zauscher, *J. Am. Chem. Soc.* **2004**, *126*, 7330; c) W. Gao, W. Liu, J. A. Mackay,

M. R. Zalutsky, E. J. Toone, A. Chilkoti, *Proc. Natl. Acad. Sci. U.S.A.* **2009**, *106*, 15231.
[27] a) D. W. Urry, T. Hugel, M. Seitz, H. E. Gaub, L. Sheiba, J. Dea, J. Xu, T. Parker, *Philos. Trans. R. Soc. London Series B-Biol. Sci.* **2002**, *357*, 169; b) W. Kim, V. P. Conticello, *Polym. Rev.* **2007**, *47*, 93.
[28] X. X. Xia, Q. Xu, X. Hu, G. Qin, D. L. Kaplan, *Biomacromolecules* **2011**, *12*, 3844.
[29] a) T. Christensen, M. Amiram, S. Dagher, K. Trabbic-Carlson, M. F. Shamji, L. A. Setton, A. Chilkoti, *Protein Sci.* **2009**, *18*, 1377; b) T. Christensen, W. Hassouneh, K. Trabbic-Carlson, A. Chilkoti, *Biomacromolecules* **2013**, *14*, 1514.
[30] a) P. Bartlett, R. H. Ottewill, *J. Chem. Phys.* **1992**, *96*, 3306; b) S. R. Kline, *J. Appl. Crystallogr.* **2006**, *39*, 895.
[31] M. Kim, S. C. Tang, B. D. Olsen, *J. Polym. Sci. Pol. Phys.* **2013**, *51*, 587.
[32] C. S. Thomas, L. Xu, B. D. Olsen, *Biomacromolecules* **2012**, *13*, 2781.
[33] C. Boutris, E. G. Chatzi, C. Kiparissides, *Polymer* **1997**, *38*, 2567.
[34] a) L. Whitmore, B. A. Wallace, *Nucleic Acids Res.* **2004**, *32*, W668; b) L. Whitmore, B. A. Wallace, *Biopolymers* **2008**, *89*, 392.